CARBON 77 (2014) 199–207

Available at www.sciencedirect.com

ScienceDirect

journal homepage: www.elsevier.com/locate/carbon

Simple and rapid micropatterning of conductive carbon composites and its application to elastic strain sensors

Jeong-Ho Kong [a], Nam-Su Jang [a], Soo-Hyung Kim [a,b], Jong-Man Kim [a,b,*]

[a] Department of Nano Fusion Technology, Pusan National University, Busan 609-735, Republic of Korea
[b] Department of Nanomechatronics Engineering, Pusan National University, Busan 609-735, Republic of Korea

ARTICLE INFO

Article history:
Received 4 March 2014
Accepted 10 May 2014
Available online 16 May 2014

ABSTRACT

The micropatterning of conductive composites is of great importance for the integration of elastic conductors with functional micro-geometries in a stretchable platform. We present a simple and rapid micropatterning method for conductive composites that relies on single-step contact transfer printing (sCTP). A conductive polydimethylsiloxane (PDMS) composite is readily synthesized by dispersing conductive carbon black nanoparticles into a PDMS matrix and is easily patterned on insulative PDMS substrates with negligible dimensional errors by the proposed method. In addition to simplicity and accuracy in fabrication, superior process scalability is revealed through investigation of both multiple-stack and large-area patterning approaches. We also demonstrate an all-elastomeric-platformed piezoresistive strain sensor capable of measuring higher tensile strains compared to conventional metal foil gauges, with highly linear, good cyclic electrical performance, and mechanical robustness. As a potential application, we integrate the strain sensors onto a glove to measure the motions of human fingers in real time. We further demonstrate a rosette-type gauge that can detect both the magnitude and direction of the principal strains with patterning accuracy and uniformity facilitated by the proposed sCTP technique.

1. Introduction

Recently, electrically conductive elastic composites (CECs) have continuously been opening up new opportunities for a range of potential applications including stretchable and flexible circuits [1–6], skin-like soft sensors [7–16], and dielectric elastic actuators [17,18]. This has been enabled by the superior advantages of CECs over their conventional stiff counterparts, such as stretchability, bendability, mechanical robustness, light weight, and low-cost fabrication. Therefore, a variety of approaches to develop CECs have been suggested, such as polymer composites with conductive nanofillers embedded and distributed spatially in polymer matrices [5,8,14,15,19–30], two-dimensional (2D) conductive nano-networks on surface areas [9,11,31–37], polymer-infiltrated three-dimensional (3D) conductive foams [38–41], and conductive films stacked or inkjet-printed onto elastic polymer substrates [7,10,12,42–46]. Of these, conductive polymer composites are one of the most attractive approaches due to their process simplicity, cost-effectiveness and tunability of the intrinsic properties such as conductivity. The composites can be simply synthesized by blending conductive nanofillers

* *Corresponding author:* Fax: +82 55 350 5289.
E-mail address: jongkim@pusan.ac.kr (J.-M. Kim).
http://dx.doi.org/10.1016/j.carbon.2014.05.022
0008-6223/

such as carbon black (CB) [8,19], carbon nanotubes (CNTs) [5,8,15,20–24], metallic particles (MPs) [19,25,26], and hybrid fillers [14,27,28] into elastomers such as polydimethylsiloxane (PDMS). In addition, the conductivity of the composites can be tailored by simply changing the nanofiller materials or their loading fraction. The patternability of the CECs is also important for expanding their applicability to practical stretchable electronics. Nevertheless, there have been only a few reports introducing micropatterning methods for CECs, and a particular lack of methods with both simplicity and accuracy in fabrication, owing the difficulty of precise manipulation of the CECs in the micro-sized regime. Several have tried to define micro- or millimeter-sized CEC patterns with shadow masks [9,11,16,23,32–34,47]. Although shadow-mask-based processes are quite simple and time-efficient, drawbacks include relatively low resolution and accuracy in patterning. Some have demonstrated CEC patterns successfully by squeezing conductive polymer composites into photolithographically defined micro-molds [8,19,48]. This approach enables the attainment of highly accurate micro-scale patterns with smaller critical dimensions compared to shadow-mask-based processes, because this patterning process is based on the well-established photolithographic technique. However, the method includes a fairly cumbersome blading process that is needed to separate the individual patterns by removing the unnecessary parts of the composites from the mold surface after squeezing. This makes the process more complicated and might also be inadequate for large-area applications. CNT ribbon patterns on elastic substrates could be obtained by drawing directly from CNT forests [42–44] or manually stacking CNT films grown from patterned catalyst layers [7]. Although aligned CNTs with a high aspect ratio could possibly be applied as stretchable conductors and strain sensors by incorporation with stretchable substrates, it is very difficult to fabricate them precisely in arbitrary shapes. Recently, some have reported unique extrusion and laser irradiation processes to fabricate piezoresistive polymeric fibers and CNT-percolated CEC patterns, respectively [29,30]. However, the approaches may suffer from difficulties in controlling critical dimensions of the resultant CEC architectures.

In this study, we demonstrate a simple and rapid strategy to fabricate micro-patterns of conductive composites in arbitrary geometries based on a single-step contact transfer printing (sCTP) technique that can be easily scaled up in both vertical (up to five-layers) and planar (up to four-inch wafer-scale) directions. The CB-doped PDMS composite is patterned selectively along micro-bumps on insulative PDMS substrates without significant distortion in the dimensions. Based on the proposed fabrication method, we realize an all-elastomeric strain sensor exhibiting linear and stable piezoresistive responses even under repetitive operations. As a practical demonstration of the elastic strain sensors, we mount them onto a glove to fabricate a device that can measure various motions of the human fingers in real time. With the superior processability of the proposed sCTP technique along with its accuracy and uniformity, we demonstrate a delta rosette gauge with the capability of sensing both the magnitude and orientation of the principal strains by fabricating three identical strain sensors oriented at 120° to each other on a substrate through a single printing.

2. Experimental details

2.1. Synthesis of conductive PDMS composites

The conductive PDMS (cPDMS) composite was prepared by simply mixing 15 wt.% conductive CB nanoparticles (Black Pearl 2000, Cabot) with liquid PDMS (Sylgard 184 Kit A, Dow Corning), as schematically represented in Fig. 1(a). Spherical CB nanoparticles with an average diameter of ~50 nm were used as conductive nanofillers because their spherical morphologies are desirable for obtaining enhanced piezoresistive behavior by enabling easy separation between individual fillers in PDMS matrix when subjected to stretching deformations. The loading concentration of CBs was experimentally optimized to 15 wt.% with considerations of both stable electrical behavior and good processability of the composites. A volatile solvent (toluene) was employed to make it easy for the CB nanoparticles to be dispersed uniformly into the highly viscous liquid PDMS. In detail, toluene solution was added to a vial containing CB nanoparticles at a weight ratio of 15:1 and the CB/toluene mixture was subsequently sonicated to disaggregate the CB nanoparticles from one another in a bath sonicator (SH-2300, SHAEHAN-SONIC) with a fixed frequency of 28 kHz for 1 h. The liquid PDMS was also diluted with the solvent at a weight ratio of 1:1 to promote easy dispersion of the CBs by reducing the viscosity of the PDMS. Each mixture (CB/toluene and PDMS/toluene) was then stirred magnetically at room temperature for 2 h, and the pre-treated two mixtures were then mixed together. The CB/PDMS/toluene mixture was magnetically stirred further in an open container on a hot plate (80 °C) under a fume hood until the volatile toluene was fully evaporated. After evaporating the solvent, the synthesis of the cPDMS composite was completed and ready to be printed by adding a curing agent (Sylgard 184 Kit B, Dow Corning) to the mixture at a weight ratio of 0.15:1.

Field emission scanning electron microscope (FESEM; S4700, HITACHI) was used to characterize the CB nanoparticles, and CB networks embedded in the PDMS matrix. Fig. 1(b) indicates that the CB nanoparticles were embedded quite uniformly into the PDMS matrix by the synthesis procedures.

2.2. Single-step contact transfer printing (sCTP)

The key micropatterning strategy of the cPDMS based on the proposed sCTP technique is illustrated schematically in Fig. 2(a). Firstly, the PDMS stamp was prepared using a micro-mold-assisted standard soft-lithographic replication process. For this, a 70-μm-thick negative-tone photoresist (PR, JSR-THB-151N) was first spin-coated on a cleaned four-inch silicon substrate at 1000 rpm and patterned by a standard photolithography process. Next, the liquid PDMS (with a weight ratio of 10:1 of base polymer and curing agent) was poured onto the mold substrate after degassing for 1 h in a desiccator connected to a vacuum pump to fully remove all the air bubbles. After curing thermally at 70 °C for 30 min, the PDMS stamp was prepared by carefully peeling off the solidified PDMS from the mold substrate. The replicated PDMS stamp was then placed on a manual z-axis stage and

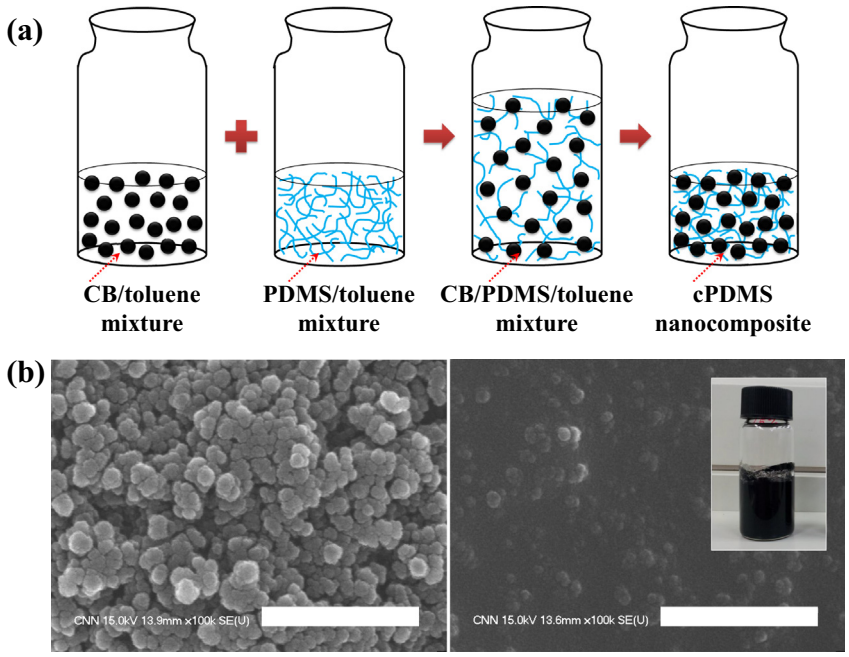

Fig. 1 – Synthesis of CB-doped conductive composites. (a) Schematic illustrations of synthesis procedures. (b) SEM images of bare CB nanoparticles (left) and CB-doped composite (right), scale bar: 500 nm (inset in right figure: synthesized composite in a vial before mixing with a curing agent). (A color version of this figure can be viewed online.)

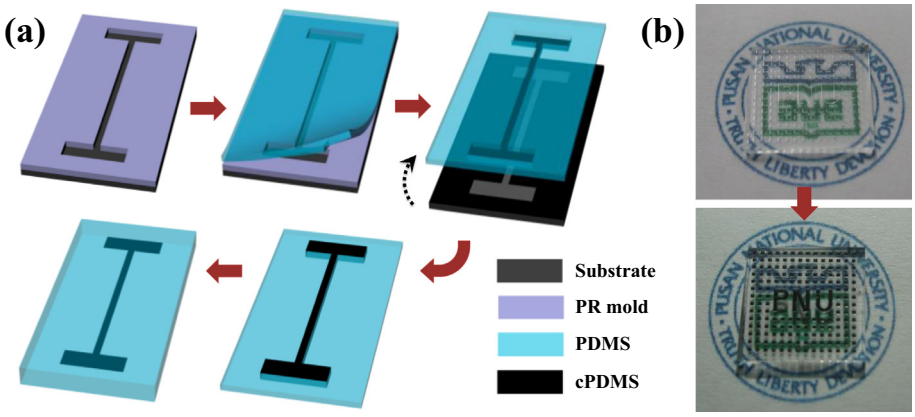

Fig. 2 – Single-step contact transfer printing (sCTP) process. (a) Schematic illustrations of fabrication procedures based on the sCTP technique. (b) As-prepared (upper) and cPDMS-printed (lower) PDMS stamp. (A color version of this figure can be viewed online.)

brought into contact with cPDMS coated onto another silicon substrate. When the PDMS stamp was raised, the cPDMS was simply patterned by selective transfer onto the surface area in contact, as shown in Fig. 2(b). Subsequently, the printed cPDMS patterns were cured thermally at 70 °C for 12 h both to solidify the cPDMS and entirely evaporate the residual solvent components. Finally, the cPDMS printed on the PDMS stamp was encapsulated by coating the liquid PDMS, followed by curing at 70 °C for 30 min.

2.3. *Characterization*

The width of the cPDMS pattern printed on the PDMS stamp was measured in at least different five regions using an optical microscope (BX60M, OLYMPUS) equipped with a CCD module. The thickness of the cPDMS pattern was obtained by subtracting the pre-measured thickness of the stamp pattern from that of the printed cPDMS layer using a 3D laser profiling system. A two-probe method was employed to measure the electrical resistance of the prepared cPDMS pattern using a digital multimeter (U1253B, Agilent Technologies).

All the stretching/releasing tests were performed at a constant loading/unloading speed of 1 mm/min using an automatic testing stand (JSV-H1000, JISC) equipped with a digital push–pull force gauge (HF-10, JISC). In all the tests, the electrical resistances were measured and recorded in real time using a digital multimeter connected to a computer with an RS-232 data cable. For the characterization of the rosette

gauge, the same measurement system was used while monitoring the resistance changes of all three strain sensors in the rosette platform simultaneously.

3. Results and discussion

3.1. Micropatterning of cPDMS composites by sCTP process

To examine the patterning accuracy of the proposed simple sCTP process, we have investigated the dimensional errors after printing with respect to the pre-defined stamp patterns. Fig. 3(a) shows the widths measured on various strip patterns of the printed cPDMS and stamp. The pattern widths of the printed cPDMS strips showed negligible dimensional errors of less than 2.5% compared to those on the stamp, as shown in Fig. 3(a). This clearly indicates that the cPDMS patterns were accurately defined only on the protruding parts of the PDMS stamp.

Fig. 3(b) shows the electrical resistance measured on the cPDMS resistors with different lengths, which were prepared on a PDMS stamp by simultaneous printing. The measured resistance was increased linearly in proportion to the resistor lengths as shown in Fig. 3(b). This linear relationship between the resistance and resistor length suggests that the changes in the electrical resistance depend only on the resistor lengths, since the PDMS stamp was initially designed for the resistors to have the same widths and the cPDMS patterns are achievable with negligible dimensional errors in width as proven in Fig. 3(a). This is clear evidence of the fact that the cPDMS patterns can also be printed without significant deviations in thickness among the adjacent patterns by the proposed sCTP technique.

Furthermore, the thickness of the cPDMS patterns can be easily programmed by controlling the number of contact transfer printings, so that the electrical properties (the conductance or resistance) can be tailored in accordance with the cPDMS thickness. Multiple printings were conducted simply by repeating the printing cycle, including a pair of contact transfer printings and subsequent curing steps. The thickness of the cPDMS was increased linearly with the increased printing number, as shown in Fig. 3(c). The thickness of the printed cPDMS was measured using a 3D laser profiler (NV-1000, Nanosystem) as 6.04 ± 1.61 μm for each printing cycle. In addition, the inset graph in Fig. 3(c) indicates that the corresponding resistance of the cPDMS pattern was decreased exponentially as the printing number was increased, which means that the pattern width was almost retained without appreciable change, even after the repeated printing cycles. Finally, the possibility of large-area patterning using the proposed sCTP technique was demonstrated by successfully printing onto a four-inch wafer-scale substrate, as shown in Fig. 3(d). It should be noted that the proposed fabrication method can potentially be combined with various types of elastic polymers

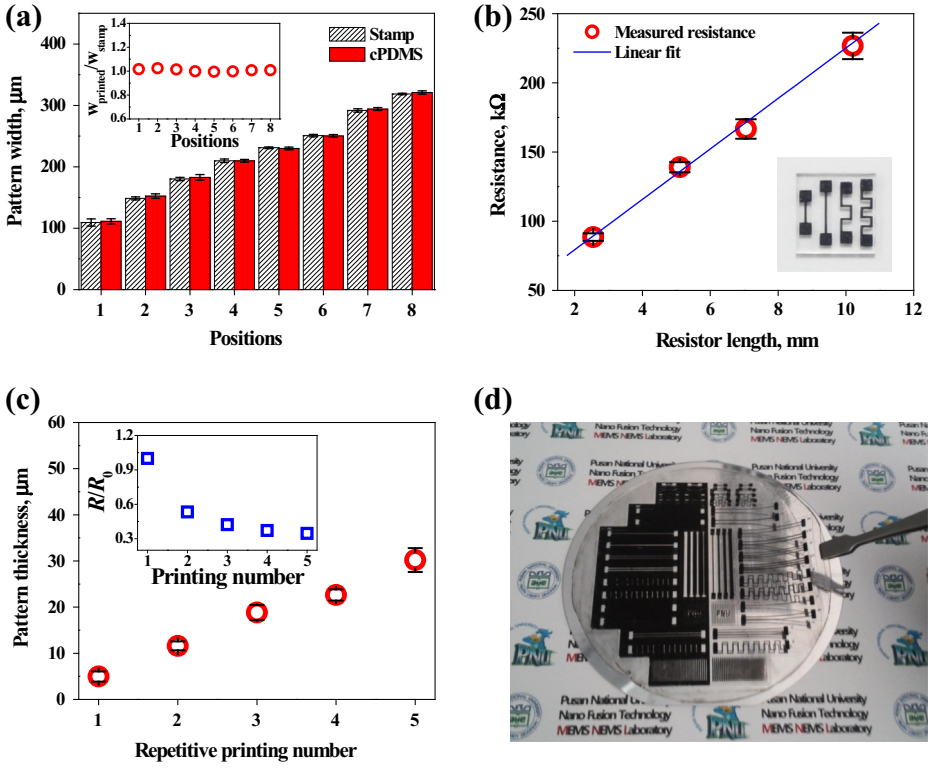

Fig. 3 – Contact transfer printing results. (a) Pattern widths measured on various strips of the printed cPDMS and stamp (inset: the ratio of the cPDMS pattern widths to those on the stamp). (b) Electrical resistance measured on cPDMS resistors with the same widths but different lengths (inset: digital image of the device under test). (c) Thickness variations of the printed cPDMS as a function of the printing number (inset: normalized electrical resistance due to repetitive printing). (d) Various cPDMS patterns printed on large-area PDMS substrate (~4 in.). (A color version of this figure can be viewed online.)

to demonstrate diverse elastic architectures that need functional micro-patterns, in a simple and low-cost manner.

3.2. *Piezoresistive elastic strain sensors*

When the cPDMS patterns are subjected to stretching deformations, their electrical properties are responsive to external loadings mainly due to the changes in the inter-distance of the adjacent CBs in the PDMS matrix. This behavior is greatly desirable for use as elastic strain sensors, which can be used to overcome the strain limits of conventional metal foil gauges (typically ~5% [7]), with the piezoresistive principle. A ribbon-shaped cPDMS strain sensor (300 μm in width and 2 cm in length) was simply fabricated using the proposed sCTP technique, and its strain gauging properties were characterized after being wired electrically.

Fig. 4(a) shows the resistance change ratio ($\Delta R/R_0$) of the fabricated sensor with respect to applied tensile strains of up to 80%, at which point the fabricated cPDMS strain sensor ruptured. The strain-dependent responses of the sensor were divided into two linear regions with the different slopes (gauge factors, GFs) at around 10% strain, as shown in Fig. 4(a). In the first region (0–10% strain), the resistance of the device was increased with a relatively steep slope (GF = ~5.5), which would be because many of the current paths (CB networks) in the PDMS matrix were lost suddenly along the strain direction. However, with more than 10% strain (the second region), the slope became lower (GF = ~1.8) compared to the first region. This decreasing tendency of the GF originates from the fact that the rate of decrease in the number of current paths in the PDMS matrix was partly alleviated by the creation of new current paths perpendicular to the strain direction, probably due to the Poisson effect (compression in the perpendicular direction). Nevertheless, these experimental observations suggest that the proposed cPDMS strain sensors can be efficiently used in a higher strain range than that of the conventional metal foil gauges, ensuring mechanical and electrical stability.

The fabricated cPDMS strain sensor exhibits a hysteretic behavior at the first loading/unloading cycle with a maximum strain of 10% due possibly to a viscoelastic property of the cPDMS (Fig. 4(b)). However, the strain-dependent responses were fully stabilized early on after a few cycles (<5 cycles) for various loading strain values, as shown in Fig. 4(c).

The inset in Fig. 4(c) shows the $\Delta R/R_0$ of the device for repetitive stretching/releasing from 21 to 30 cycles, which clearly indicates that the resistance at stretching returned perfectly to its starting value, having increased by ~10% with respect to the initial resistance (R_0), without hysteresis for each cycle under 10% tensile strain after stabilization.

Fig. 4(d) shows the resistance change ratios obtained from the three identical strain sensors, which were fabricated independently under the same sCTP conditions, after a few transient cycles. The resistive behaviors for each sensor were

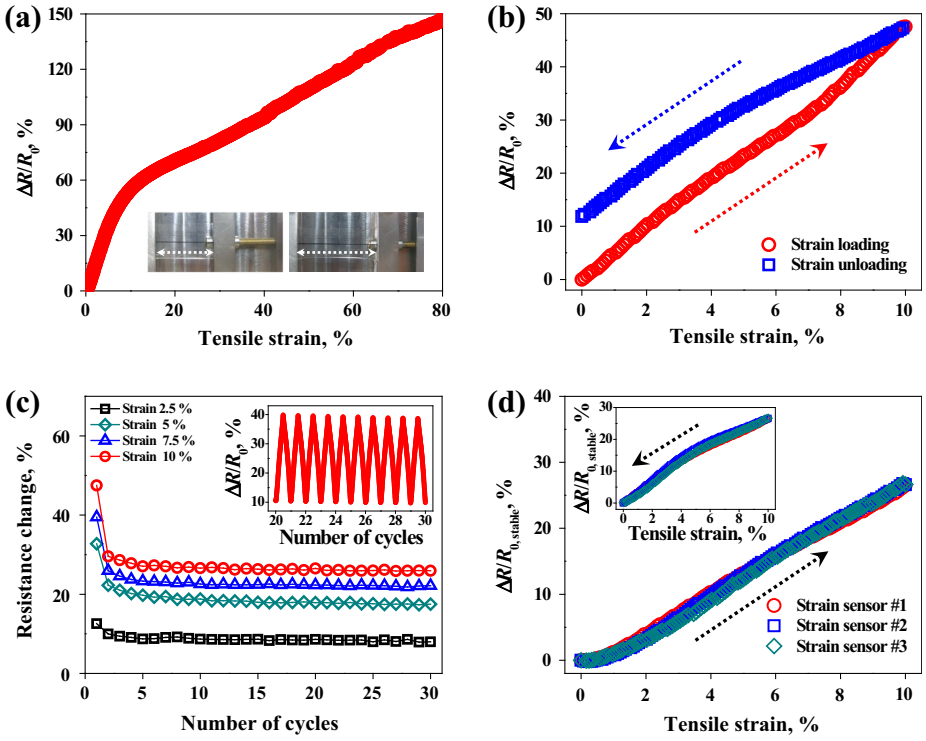

Fig. 4 – Performance evaluations of ribbon-shaped piezoresistive cPDMS strain sensor. (a) Resistance change ratio ($\Delta R/R_0$) under the applied tensile strain of up to 80%. (b) $\Delta R/R_0$ at first stretching/releasing cycle with a maximum strain of 10%. (c) Resistance change ratio for each stretching/releasing cycle of up to 30 cycles (inset: $\Delta R/R_0$ due to repetitive stretching/releasing from 21 to 30 cycles with application of 10% strain). (d) Resistance change ratios of three identical cPDMS strain sensors with a maximum strain of 10% after stabilization (inset: resistance change ratios of the devices during releasing). (A color version of this figure can be viewed online.)

quite uniform with little deviation both upon stretching and subsequent release, as shown in Fig. 4(d). These experimental results demonstrate another advantage of the proposed sCTP technique in terms of reproducibility.

The potential of the cPDMS strain sensor in practical wearable applications was simply demonstrated by monitoring the motions of human fingers with a motion sensing glove in real time, as shown in Fig. 5. A motion sensing glove was first prepared by assembling the fabricated cPDMS strain sensors on each finger joint of the glove using Velcro fasteners at both ends of the device. Fig. 5(a) shows the changes in electrical resistance for cyclic bending and straightening motions of the finger, which indicates that the resistance was immediately increased with the applied bending deformation, and it recovered gradually to its initial value at straightening. Moreover, the magnitude of the resistance change ratio could be clearly determined depending on the degree of finger bending, as shown in Fig. 5(a). In addition, the cPDMS strain sensor worn on the finger could readily react with even slight bending of the knuckle such as, with single and double click motions with a computer mouse, as shown in Fig. 5(b). Furthermore, independent gestures of the five fingers could also be easily detected with five individual cPDMS strain sensors mounted on the motion-sensing glove.

Fig. 5(c) shows the resultant resistance changes with respect to the sequential motions of the individual fingers as a function of time. The motion sequences comprised the following: (1) rest → (2) the thumb bending and holding → (3) the middle finger bending and holding → (4) the ring finger bending and holding → (5) the ring finger straightening → (6) the middle finger straightening → (7) the thumb straightening. It is worthy to note that the cPDMS strain sensors functioned stably even after much repetitive bending and straightening cycles of the fingers, thus demonstrating mechanical durability in practical use.

3.3. *Rosette-type gauge applications*

A single strain sensor is generally capable only of detecting the strain in the operating direction to which the device is aligned. To overcome the direction dependence of single strain sensors, we demonstrated a delta rosette-type gauge that can simultaneously measure the magnitude and direction of the principal strains by arranging three independent serpentine-shaped strain sensors oriented at a fixed angle of 120° with respect to each other. The principal strains and principal angle can be readily obtained by solving the well-known strain transformation equations with the strains measured on the three serpentine strain sensors in the rosette configuration [49].

Fig. 6(a) shows the fabricated rosette-configured gauge indicating the direction of the major principal strain. Each independent strain sensor is denoted as S_1, S_2, and S_3 in the figure. To investigate the response characteristics of the fabricated rosette gauge under stretching, tensile strain was applied along the axis aligned to the operating direction of S_1, which means that the principal angle was pre-defined as 0°. Fig. 6(b) shows the resistance change ratio measured simultaneously on the independent strain sensors with the application of tensile strain of up to 5%. The changes in the electrical resistance of all the independent strain sensors were found to be highly linear with respect to the applied strain, and the resistance change of S_1 was dominantly larger than those of the others as shown in Fig. 6(b).

In principle, the equations for calculating the principal strains and principal angle in the rosette gauge can be derived

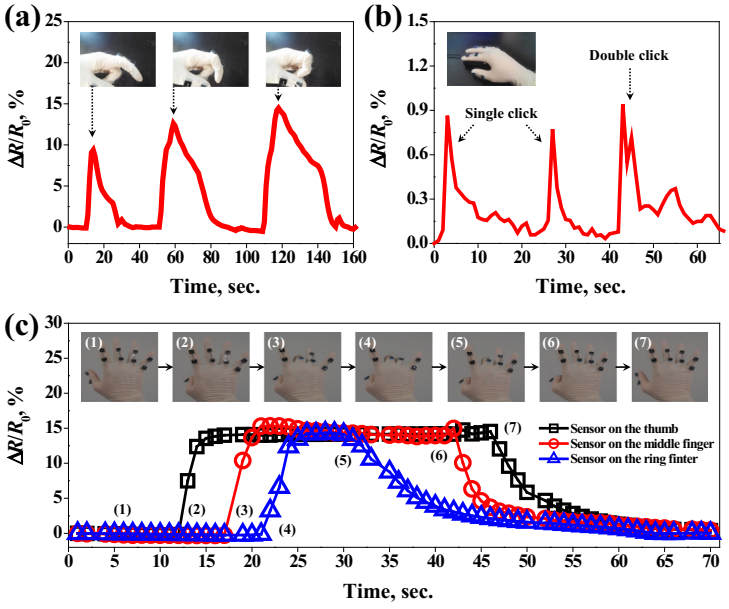

Fig. 5 – Potential wearable applications of cPDMS strain sensor (motion sensing glove). (a) Resistance change ratio ($\Delta R/R_0$) due to repetitive bending and straightening motions of the finger with different levels of finger bending. (b) $\Delta R/R_0$ due to mouse click motions (single and double click). (c) $\Delta R/R_0$ due to independent series gestures of the five fingers (all the insets: digital images for the finger motions corresponding to resultant resistance changes). (A color version of this figure can be viewed online.)

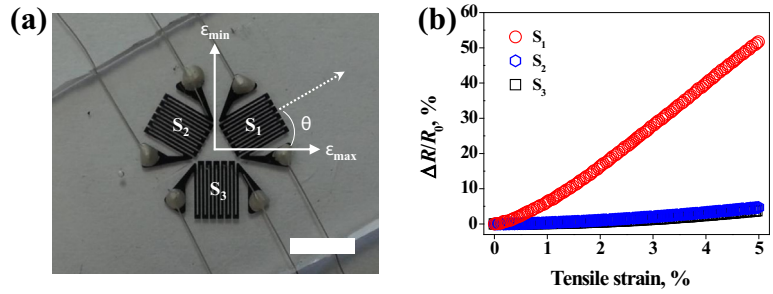

Fig. 6 – cPDMS delta rosette gauge. (a) Fabricated rosette-configured gauge indicating the direction of the major principal strain (scale bar: 5 mm). (b) Resistance change ratios of the three independent strain sensors in the rosette platform with respect to the applied strain of 5%. (A color version of this figure can be viewed online.)

from the strain transformation relationship, which can also be readily visualized with the help of Mohr's circle. The normal strain at any angle, φ, from the major principal axis can be represented in its simplest form as follows:

$$\varepsilon_\varphi = \frac{\varepsilon_{max} + \varepsilon_{min}}{2} + \frac{\varepsilon_{max} - \varepsilon_{min}}{2} \cos 2\varphi \quad (1)$$

where ε_{max} and ε_{min} are the maximum and minimum principal strains, respectively.

Assuming that a reference strain sensor (S_1) in the delta rosette configuration is oriented at an angle of θ with respect to the direction of the major principal strain, as shown in Fig. 6(a), the normal strains of each independent strain sensor ($\varepsilon_1, \varepsilon_2,$ andε_3 for S_1, S_2, and S_3, respectively) can be represented by substituting their corresponding angles, θ, $\theta + 60°$, and $\theta + 120°$, into Eq. (1) as follows:

$$\varepsilon_1 = \frac{\varepsilon_{max} + \varepsilon_{min}}{2} + \frac{\varepsilon_{max} - \varepsilon_{min}}{2} \cos 2\theta \quad (2a)$$

$$\varepsilon_2 = \frac{\varepsilon_{max} + \varepsilon_{min}}{2} + \frac{\varepsilon_{max} - \varepsilon_{min}}{2} \cos 2(\theta + 60°) \quad (2b)$$

$$\varepsilon_3 = \frac{\varepsilon_{max} + \varepsilon_{min}}{2} + \frac{\varepsilon_{max} - \varepsilon_{min}}{2} \cos 2(\theta + 120°) \quad (2c)$$

The principal strains and principal angle can be represented by arranging Eq. (2) in terms of the strains, ε_1, ε_2, and ε_3 as follows:

$$\varepsilon_{max} = \frac{\varepsilon_1 + \varepsilon_2 + \varepsilon_3}{3} + \frac{\sqrt{2}}{3}\sqrt{(\varepsilon_1 - \varepsilon_2)^2 + (\varepsilon_2 - \varepsilon_3)^2 + (\varepsilon_3 - \varepsilon_1)^2} \quad (3a)$$

$$\varepsilon_{min} = \frac{\varepsilon_1 + \varepsilon_2 + \varepsilon_3}{3} - \frac{\sqrt{2}}{3}\sqrt{(\varepsilon_1 - \varepsilon_2)^2 + (\varepsilon_2 - \varepsilon_3)^2 + (\varepsilon_3 - \varepsilon_1)^2} \quad (3b)$$

$$\theta = \frac{1}{2}\tan^{-1}\left(\frac{\sqrt{3}(\varepsilon_2 - \varepsilon_3)}{2\varepsilon_1 - \varepsilon_2 - \varepsilon_3}\right) \quad (4)$$

When the rosette gauge is subjected to any strain state, the magnitude and direction of the principal strains in response to the strain can be obtained by Eqs. (3) and (4), since the strains, ε_1, ε_2, and ε_3, on the right-hand side can be experimentally measured from each independent strain sensor in the rosette configuration.

The strain values of the independent strain sensors, S_1, S_2, and S_3, were derived from the measured resistance change ratios with respect to the external strain of 5% as 51.7%, 4.7%, and 3.7%, respectively. The maximum principal strain, minimum principal strain, and principal angle of the rosette system were calculated by substituting the strain values of the three strain sensors for the strain transformation equations, and obtained accordingly as 4.75%, −1.07%, and 0.01°, respectively. The magnitude and direction of the maximum principal strain derived from the strain transformation equations showed good consistency with those of the applied strain without significant discrepancies. This clearly suggests that the cPDMS rosette gauge is highly applicable to diverse practical fields due to the precise and simultaneous sensing capability of both magnitude and direction of the principal strains. This also demonstrates that the proposed sCTP technique is useful for fabricating the rosette architecture by enabling simultaneous patterning of the three sensing components and probing electrodes in a precise and uniform manner.

4. Conclusions

A simple and accurate route to embed arbitrarily shaped micro-scale cPDMS patterns onto elastomeric platforms based on a single-step contact transfer printing (sCTP) technique has been proposed. The simple fabrication approach is able to control the electrical properties of the printed cPDMS pattern in a linear manner by simply changing its thickness by varying the number of printings. The technique is highly applicable for scaling up toward large-area fabrication, which has been demonstrated for a wafer of up to 4 in. in size. In this way, we have fabricated a highly elastic strain sensor based on the piezoresistive effect enabled by the CB-doped PDMS. This all-elastomeric sensor architecture makes it possible for the device to be robust against stretching, bending, and twisting deformations. The piezoresistive responses of the fabricated cPDMS strain sensors are revealed to be highly linear up to 10% tensile strain and fully stabilized without significant hysteretic behavior after transient cycles. Moreover, several strain sensors fabricated independently using the same sCTP conditions showed uniform response characteristics in both stretching and releasing with a maximum tensile strain of up to 10% after stabilization. Various motions of the human fingers were successfully monitored in real time by demonstrating a motion-sensing glove integrated with several identical cPDMS strain sensors. In addition, we have demonstrated a rosette-configured gauge capable of detecting

both the magnitude and direction of the principal strains with high sensing accuracy. The proposed sCTP technique is highly feasible for use as a promising fabrication route for future stretchable electronics owing to its superior advantages, which include simplicity, accuracy, scalability, cost-effectiveness, and uniformity in fabrication.

Acknowledgments

This research was supported by the Civil & Military Technology Cooperation Program through the National Research Foundation of Korea (NRF) funded by the Ministry of Science, ICT & Future Planning (No. 2013M3C1A9055407). This work was also supported by the Industry-University Co-Innovation Project, Republic of Korea.

REFERENCES

[1] Rogers JA, Someya T, Huang Y. Materials and mechanics for stretchable electronics. Science 2010;327:1603–7.
[2] Sekitani T, Someya T. Stretchable, large-area organic electronics. Adv Mater 2010;22:2228–46.
[3] Ahn J-H, Je JH. Stretchable electronics: materials, architectures and integrations. J Phys D 2012;45:103001.
[4] Park S-I, Le A-P, Wu J, Huang Y, Li X, Rogers JA. Light emission characteristics and mechanics of foldable inorganic light-emitting diodes. Adv Mater 2010;22:3062–6.
[5] Sekitani T, Nakajima H, Maeda H, Fukushima T, Aida T, Hata K, et al. Stretchable active-matrix organic light-emitting diode display using printable elastic conductors. Nat Mater 2009;8:494–9.
[6] Park M, Im J, Shin M, Min Y, Park J, Cho H, et al. Highly stretchable electric circuits from a composite material of silver nanoparticles and elastomeric fibres. Nat Nanotechnol 2012;7:803–9.
[7] Yamada T, Hayamizu Y, Yamamoto Y, Yomogida Y, Izadi-Najafabadi A, Futaba DN, et al. A stretchable carbon nanotube strain sensor for human-motion detection. Nat Nanotechnol 2011;6:296–301.
[8] Lu N, Lu C, Yang S, Rogers J. Highly sensitive skin-mountable strain gauges based entirely on elastomers. Adv Funct Mater 2012;22:4044–50.
[9] Cohen DJ, Mitra D, Peterson K, Maharbiz MM. A highly elastic, capacitive strain gauge based on percolating nanotube networks. Nano Lett 2012;12:1821–5.
[10] Li X, Zhang R, Yu W, Wang K, Wei J, Wu D, et al. Stretchable and highly sensitive graphene-on-polymer strain sensors. Sci Rep 2012;2:870.
[11] Wang X, Li T, Adams J, Yang J. Transparent, stretchable, carbon-nanotube-inlaid conductors enabled by standard replication technology for capacitive pressure, strain and touch sensors. J Mater Chem A 2013;1:3580–6.
[12] Bae S-H, Lee Y, Sharma BK, Lee H-J, Kim J-H, Ahn J-H. Graphene-based transparent strain sensor. Carbon 2013;51:236–42.
[13] Cai L, Song L, Luan P, Zhang Q, Zhang N, Gao Q, et al. Super-stretchable, transparent carbon nanotube-based capacitive strain sensors for human motion detection. Sci Rep 2013;3:3048.
[14] Lee C, Jug L, Meng E. High strain biocompatible polydimethylsiloxane-based conductive graphene and multiwalled carbon nanotube nanocomposite strain sensors. Appl Phys Lett 2013;102:183511.
[15] Sekitani T, Noguchi Y, Hata K, Fukushima T, Aida T, Someya T. A rubberlike stretchable active matrix using elastic conductors. Science 2008;321:1468–72.
[16] Lipomi DJ, Vosgueritchian M, Tee BC-K, Hellstrom SL, Lee JA, Fox CH, et al. Skin-like pressure and strain sensors based on transparent elastic films of carbon nanotubes. Nat Nanotechnol 2011;6:788–92.
[17] Pelrine R, Kornbluh R, Pei Q, Joseph J. High-speed electrically actuated elastomers with strain greater than 100%. Science 2000;287:836–9.
[18] Pelrine R, Kornbluh R, Kofod C. High-strain actuator materials based on dielectric elastomers. Adv Mater 2000;12:1223–5.
[19] Niu X, Peng S, Liu L, Wen W, Sheng P. Characterizing and patterning of PDMS-based conducting composites. Adv Mater 2007;19:2682–6.
[20] Lee H, Yoo J-K, Park J-H, Kim JH, Kang K, Jung YS. A stretchable polymer-carbon nanotube composite electrode for flexible lithium-ion batteries: porosity engineering by controlled phase separation. Adv Energy Mater 2012;2:976–82.
[21] Ata S, Kobashi K, Yumura M, Hata K. Mechanically durable and highly conductive elastomeric composites from long single-walled carbon nanotubes mimicking the chain structure of polymers. Nano Lett 2012;12:2710–6.
[22] Huang YY, Terentjev EM. Tailoring the electrical properties of carbon nanotube-polymer composites. Adv Funct Mater 2010;20:4062–8.
[23] Liu C-X, Choi J-W. Precision patterning of conductive polymer nanocomposite using a laser-ablated thin film. J Micromech Microeng 2012;22:045014.
[24] Zhang R, Deng H, Valenca R, Jin J, Fu Q, Bilotti E, et al. Carbon nanotube polymer coatings for textile yarns with good strain sensing capability. Sens Actuators A 2012;179:83–91.
[25] Li Z, Zhang R, Moon K-S, Liu Y, Hansen K, Le T, et al. Highly conductive, flexible, polyurethane-based adhesives for flexible and printed electronics. Adv Funct Mater 2013;23:1459–65.
[26] Araki T, Nogi M, Suganuma K, Kogure M, Kirihara O. Printable and stretchable conductive wirings comprising silver flakes and elastomers. IEEE Electron Device Lett 2011;32:1424–6.
[27] Chun K-Y, Oh Y, Rho J, Ahn J-H, Kim Y-J, Choi HR, et al. Highly conductive, printable and stretchable composite films of carbon nanotubes and silver. Nat Nanotechnol 2010;5:853–7.
[28] Chun K-Y, Kim SH, Shin MK, Kim YT, Spinks GM, Aliev AE, et al. Free-standing nanocomposites with high conductivity and extensibility. Nanotechnology 2013;24:165401.
[29] Cravanzola S, Haznedar G, Scarano D, Zecchina A, Cesano F. Carbon-based piezoresistive polymer composites: structure and electrical properties. Carbon 2013;62:270–7.
[30] Cesano F, Rattalino I, Demarchi D, Bardelli F, Sanginario A, Gianturco A, et al. Structure and properties of metal-free conductive tracks on polyethylene/multiwalled carbon nanotube composites as obtained by laser stimulated percolation. Carbon 2013;61:63–71.
[31] Shin MK, Oh J, Lima M, Kozlov ME, Kim SJ, Baughman RH. Elastomeric conductive composites based on carbon nanotube forests. Adv Mater 2010;22:2663–7.
[32] Xu F, Zhu Y. Highly conductive and stretchable silver nanowire conductors. Adv Mater 2012;24:5117–22.
[33] Lee P, Lee J, Lee H, Yeo J, Hong S, Nam KH, et al. Highly stretchable and highly conductive metal electrode by very long metal nanowire percolation network. Adv Mater 2012;24:3326–32.
[34] Akter T, Kim WS. Reversibly stretchable transparent conductive coatings of spray-deposited silver nanowires. ACS Appl Mater Interfaces 2012;4:1855–9.

[35] Ho X, Tey JN, Liu W, Cheng CK, Wei J. Biaxially stretchable silver nanowire transparent conductors. J Appl Phys 2013;113:044311.
[36] Yun S, Niu X, Yu Z, Hu W, Brochu P, Pei Q. Compliant silver nanowire-polymer composite electrodes for bistable large strain actuation. Adv Mater 2012;24:1321–7.
[37] Hu W, Niu X, Li L, Yun S, Yu Z, Pei Q. Intrinsically stretchable transparent electrodes based on silver-nanowire-crosslinked-polyacrylate composites. Nanotechnology 2012;23:344002.
[38] Chen Z, Ren W, Gao L, Liu B, Pei S, Cheng H-M. Three-dimensional flexible and conductive interconnected graphene networks grown by chemical vapour deposition. Nat Mater 2011;10:424–8.
[39] Park J, Wang S, Li M, Ahn C, Hyun JK, Kim DS, et al. Three-dimensional nanonetworks for giant stretchability in dielectrics and conductors. Nat Commun 2012;3:916.
[40] Ge J, Yao H-B, Wang X, Ye Y-D, Wang J-L, Wu Z-Y, et al. Stretchable conductors based on silver nanowires: improved performance through a binary network design. Angew Chem Int Ed 2013;52:1654–9.
[41] Gui X, Cao A, Wei J, Li H, Jia Y, Li Z, et al. Soft, highly conductive nanotube sponges and composites with controlled compressibility. ACS Nano 2010;4:2320–6.
[42] Liu K, Sun Y, Liu P, Lin X, Fan S, Jiang K. Cross-stacked superaligned carbon nanotube films for transparent and stretchable conductors. Adv Funct Mater 2011;21:2721–8.
[43] Zhang Y, Sheehan CJ, Zhai J, Zou C, Luo H, Xiong J, et al. Polymer-embedded carbon nanotube ribbons for stretchable conductors. Adv Mater 2010;22:3027–31.
[44] Xu F, Wang X, Zhu Y, Zhu Y. Wavy ribbons of carbon nanotubes for stretchable conductors. Adv Funct Mater 2012;22:1279–83.
[45] Chung S, Lee J, Song H, Kim S, Jeong J, Hong Y. Inkjet-printed stretchable silver electrode on wave structured elastomeric substrate. Appl Phys Lett 2011;98:153110.
[46] Lee J, Chung S, Song H, Kim S, Hong Y. Lateral-crack-free, buckled, inkjet-printed silver electrodes on highly pre-stretched elastomeric substrates. J Phys D 2013;46:105305.
[47] Wang X, Hu H, Shen Y, Zhou X, Zheng Z. Stretchable conductors with ultrahigh tensile strain and stable metallic conductance enabled by prestrained polyelectrolyte nanoplatforms. Adv Mater 2011;23:3090–4.
[48] Gutierrez CA, Meng E. Low-cost carbon thick-film strain sensors for implantable applications. J Micromech Microeng 2010;20:095028.
[49] Gere JM, Timoshenko SP. Mechanics of materials. Boston: PWS Publishing Company; 1997.